IEEE Access
Multidisciplinary | Rapid Review | Open Access Journal

Received February 6, 2021, accepted March 8, 2021, date of publication March 17, 2021, date of current version March 29, 2021.

Digital Object Identifier 10.1109/ACCESS.2021.3066003

MAS-Based Slip Ratio Fault-Tolerant Control in Finite Time for EV

NIAONA ZHANG[1,3], ZONGZHI HAN[1,2], ZHE ZHANG[2,3], KONGHUI GUO[2,3], AND XIAOHUI LU[1,2]

[1]School of Electrical and Electronic Engineering, Changchun University of Technology, Changchun 130012, China
[2]State Key Laboratory of Automotive Simulation and Control, Jilin University, Changchun 130022, China
[3]KH Automotive Technologies Company Ltd., Changchun 130012, China

Corresponding authors: Xiaohui Lu (luxh13@ccut.edu.cn) and Niaona Zhang (zhangniaona@ccut.edu.cn)

This work was supported in part by the National Natural Science Foundation of China under Grant U1864206, in part by the National Key Research and Development Plan of China under Grant 2017YFB0103600 and Grant 2017YFB0103700, and in part by the Science and Technology Development Plan of Jilin Province under Grant 2019C040-5, Grant 20180519014JH, and Grant 20200201057JC.

ABSTRACT The driving torques of all four wheels of distributed drive electric vehicles are independently controllable, and acceleration slip regulation (ASR) can be realized through the coordinated effort of torque actuators. Considering the multiple actuator coupling, nonlinearity, uncertainty and actuator faults in an ASR system, an adaptive nonsingular terminal sliding mode (NTSM) fault-tolerant control method-based multi-agent system (MAS) is proposed to address the above problems of an ASR system in this paper. First, based on multi-agent theory, a four- wheel independent drive ASR system is decomposed into four separate driving wheel agent systems to reduce the model dimension and transform the design of the ASR system controller into the design of a single driving wheel agent controller to reduce the computational complexity. Second, to address the unknown uncertainty of an actuator fault in an ASR system, an adaptive NTSM controller for a single driving wheel agent is designed to make the actual slip ratio track the ideal slip ratio for the ASR system in finite time. The controller switch item gains are selected by using an adaptive estimation mechanism for a single driving wheel agent controller to address the gain overestimation problem. This approach ensures that the actual control signal is smooth and that chattering phenomena and energy consumption are reduced. For actuator faults, a Lyapunov function based on multiagent theory is designed for a single driving wheel agent to avoid the impact of the coupling subsystem fault. Third, the Simulink and CarSim cosimulation results show that the proposed method improves the fault tolerance and robustness. The system can realize the actual slip ratio, track the optimal slip ratio in a finite time under different road adhesion conditions and effectively avoid the wheel slippage problem.

INDEX TERMS Four-wheel drive (4WD) electric vehicles (EV), acceleration slip regulation (ASR), multiagent system (MAS), slip ratio, terminal sliding mode control, adaptive sliding mode, fault-tolerant control (FTC).

I. INTRODUCTION

Compared with traditional internal combustion engine vehicles, distributed-drive electric vehicles eschew complex traditional systems, such as transmissions and differentials, to attain higher transmission efficiency. Moreover, the drive motors of each wheel can be controlled independently. The performance and stability of distributed-drive electric vehicles depend to a large extent on the proper operation of four distinct wheel motors. However, distributed-drive electric vehicles are a highly nonlinear system with strong coupling and time-varying parameters, so the control of vehicle dynamics has become a challenging research topic.

The anti-skid control system of distributed-drive electric vehicles is realized by adjusting the driving force of the driving wheels to maintain the wheel slip ratio within an optimal range. Therefore, the wheels demonstrate relatively robust adhesion during the acceleration process to prevent the car from slipping during starting and accelerating. Therefore, the safety of the vehicle is effectively improved during acceleration. At present, both domestic and foreign scholars have proposed a series of control methods for anti- skid control systems.

The associate editor coordinating the review of this manuscript and approving it for publication was Yilun Shang.

A robust nonlinear model predictive control strategy for torque distribution was proposed that guaranteed stability in the presence of uncertainties and state constraints [1]–[3]. A hierarchical control method was proposed to highly improve the lateral stability of vehicles under extreme conditions while conserving tire slip energy [4], [5]. An accelerated slip adjustment algorithm based on fuzzy logic was proposed to maintain the wheel slip ratio in an optimal range [6], [7]. An active neuro-fuzzy wheel slippage control was proposed in the longitudinal direction of a commercial vehicle [8]. A preallocation law, a multi objective optimization based on mathematical programming and a model-based range extension control were proposed as a wheel torque distribution strategy for energy efficiency optimization [9]– [11]. A wheel slippage controller based on a sliding mode was proposed for an ABS system and an ASR system, and the braking force was maximized by regulating the wheel slip ratio to maintain directional stability [12]–[14]. An adaptive sliding mode control was proposed and parametric and modeling uncertainties were estimated by adaptive neural networks and fuzzy algorithms to reduce chattering [15]–[17]. To achieve a simultaneous adhesion limit for front and rear axle wheels, the driving force and braking force were distributed [18]. The performance of selected traction controllers from the literature was compared, and focus was placed on proportional integral (PI), sliding-mode PI, integral sliding mode control and H∞ control techniques [19], [20].The performance of alternative objective functions was assessed for the optimal wheel torque distribution in an offline optimization procedure [21].

Distributed-drive electric vehicles have redundant actuators. This increase in the number of actuators also increases the probability of actuator failure. This in-wheel motor failure may be caused by mechanical failure, an overheated motor, or a failure related to the motor drive. In the case of actuator failure, if there is no suitable adjustment strategy, the performance of the vehicle may become unsatisfactory or unstable. At present, domestic and foreign scholars have proposed a series of actuator fault-tolerant control methods. For the active fault tolerance of electric vehicles, a multi input and multioutput model-free adaptive control in [22] and a modified FT finite control set model predictive control in [23] were proposed. A robust H-infinity output feedback controller was developed to address the problem of active suspension control with actuator faults and time delays [24]. A Kalman filter and a sliding mode observer were used for actuator fault-tolerant control through the reconstruction of the control law [25]–[27]. A fault-tolerant torque controller based on sliding mode control in [28], [29] and an adaptive sliding mode fault-tolerant coordination control in [30] was presented to address multi motor coordinate operation against actuator faults in a 4WID system.

Compared to the abovementioned approaches, variable structure systems are well known for their robustness in system parameter variations and external disturbances. The dynamic behavior of a system can be determined by a particular choice of switching manifolds. Compared with the linear sliding mode, the terminal sliding mode offers the advantages of fast dynamic response, finite time convergence and high steady-state accuracy by introducing nonlinear terms into the sliding mode, which is especially suitable for high-precision system control. However, in sliding mode control, the chattering caused by discontinuous switching items due to the sign function will consume system energy, exacerbate high-frequency unmodeled dynamics and minimize system performance. At present, domestic and foreign scholars have proposed methods to suppress chattering. Adaptive algorithms, interference observers, and neural networks have been used to approximate interference online to reduce switching item gains [31], [14]–[17]. The alternating effect of three sliding mode surfaces was used to reduce the switching frequency of the control law [32]. Improved approaching laws in [33]–[34] and new sliding mode surface functions in [35], [36] were designed to reach the sliding mode surface quickly and reduce the chattering phenomenon effectively. Other methods have also been used to suppress chattering, such as multi objective optimization sliding modes [37] and high-order sliding mode controls [38]. Therefore, suppressing chatter at a low cost and ensuring the accuracy of sliding mode control at the same time are worthy of study. For T-S fuzzy-model-based nonlinear Markovian jump singular systems subject to matched/unmatched uncertainties, a novel integral-type fuzzy sliding surface is proposed, which the matched uncertainties are completely compensated, and the unmatched ones are not amplified during sliding motion [39], [40].

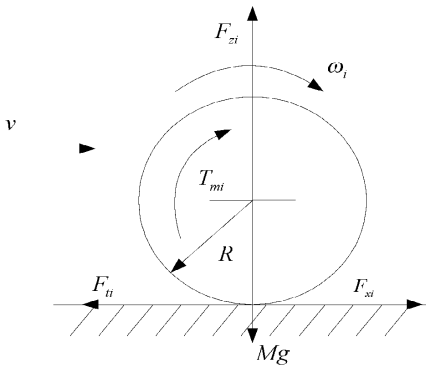

FIGURE 1. The system model of the driving wheel.

According to the characteristics of independent and controllable driving torque of four wheels distributed electric vehicles, considering communication connection and hardware topology of four wheels, the mathematical model of each wheel of anti-skid drive system based on graph theory was firstly established to reduce the complexity of ASR system modeling and improve computational efficiency. Then, according to the state information of each wheel agent and adjacent agents, an NTSM fault-tolerant control method based on multi-agent theory is proposed. The switching gain of the controller can be adjusted adaptively to compensate the influence of uncertainty and external interference in the

system and avoid buffeting and high energy consumption caused by overestimation of gain. When the actuator of the wheel agent failures, the Lyapunov function is designed based on the multi-agent theory, and the parameters of the controller are adjusted adaptively according to the failure situation, so that each wheel agent can still track the optimal slip ratio in limited time under different road adhesion conditions and actuator failures. It can effectively improve the robustness, adaptability and fault tolerance of ASR system for distributed drive electric vehicle.

II. THE ASR SYSTEM MODEL OF A DISTRIBUTED DRIVE ELECTRIC VEHICLE

A. VEHICLE DYNAMICS MODEL

During the vehicle driving process, the anti-slip control of a single wheel level can be realized. The dynamic system model of a single driving wheel is shown in Fig.1.

In the Fig.1, F_{ti}, T_{mi}, F_{xi} and F_{zi} are the resistance force generated from the ground, the motor driving torque, the longitudinal force, and the normal reaction force generated by the ground of the i th wheel, respectively, and $i = 1, 2, 3,$ or 4. Mg, R, ω and v are the gravity force of the vehicle, the rolling radius of the wheel, the wheel angular velocity, and the longitudinal velocity of the vehicle, respectively. When the driving force exceeds the maximum value of the attachment condition limit, the wheel will slip. The slip ratio of the ith driving wheel agent is defined as follows:

$$s_{di} = \frac{R\omega_i - v_i}{R\omega_i} \tag{1}$$

ω_i and v_i are the wheel angular velocity and the longitudinal velocity of the ith driving wheel agent, respectively.

The front and rear axles of the load change are converted into the load variations of a single wheel:

$$\begin{aligned} F_{z1} &= F_{z2} = M \cdot g \cdot \frac{b}{L} - M \cdot a_x \cdot \frac{h}{L} \\ F_{z3} &= F_{z4} = M \cdot g \cdot \frac{a}{L} + M \cdot a_x \cdot \frac{h}{L} \end{aligned} \tag{2}$$

where M and a_x are one quarter of the mass belonging to the vehicle and the centroid longitudinal acceleration of the vehicle, and a, b, L and h are the length from the centroid to the front axle, the length from the centroid to the rear axle, the axial length and the height of centroid, respectively.

The driving force of the electric vehicle is greater than the adhesion between the driving wheel and the road surface, which is the direct cause of the acceleration slippage of the electric vehicle. To prevent the driving wheels from slipping, it is necessary to control the driving torque distribution and reduce the driving force of electric vehicle appropriately.

The ground tangential reaction force generated by the driving torque provided by the vehicle to the wheel must be greater than the adhesion force and can be expressed by the following formula:

$$F_{xi} \le \mu_i F_{zi} \tag{3}$$

The dynamics equation of the wheel motion is as follows:

$$I\dot{\omega}_i = T_{mi} - F_{xi}R, \quad i = 1, 2, 3, 4 \tag{4}$$

where I represents the rotation inertia of the i th wheel.

B. TIRE MODEL

Under different tire and road surface adhesion conditions, the optimal slip ratio corresponding to the maximum adhesion coefficient of the tire is not the same. In the control tracking of the optimal slip ratio, the tire uses the experimental parameters of the known tire model and derives the optimal slip rate under different typical road conditions. To facilitate the analysis and research, this paper adopts the Burckhardt tire model with simple structure and practicality and uses the model parameters to obtain the optimal slip rate under different road surfaces. The mathematical expression of the Burckhardt tire is as follows:

$$\mu_i = c_1\left[1 - e^{-c_2 s_{di}}\right] - c_3 s_{di} \tag{5}$$

where c_1, c_2 and c_3 are the fitting factors, and the value of the specific tires is related to the road surface adhesion conditions.

C. TORQUE DISTRIBUTION

Without considering the rolling friction and wind resistance, the ground tangential reaction force generated by the wheel defined is equal to the adhesion force. Substituting equations (2), (3) and (5) into Equation (4) can be obtained as follows:

$$\begin{cases} T_{m1} = I\dot{\omega}_1 + \left\{c_1 \cdot \left(1 - e^{-c_2 s_{d1}}\right) - c_3 s_{d1}\right\} \\ \quad \cdot \left(M \cdot g \cdot \frac{b}{L} - M \cdot a_x \cdot \frac{h}{L}\right) \cdot R \\ T_{m2} = I\dot{\omega}_2 + \left\{c_1 \cdot \left(1 - e^{-c_2 s_{d2}}\right) - c_3 s_{d2}\right\} \\ \quad \cdot \left(M \cdot g \cdot \frac{b}{L} - M \cdot a_x \cdot \frac{h}{L}\right) \cdot R \\ T_{m3} = I\dot{\omega}_3 + \left\{c_1 \cdot \left(1 - e^{-c_2 s_{d3}}\right) - c_3 s_{d3}\right\} \\ \quad \cdot \left(M \cdot g \cdot \frac{a}{L} + M \cdot a_x \cdot \frac{h}{L}\right) \cdot R \\ T_{m4} = I\dot{\omega}_4 + \left\{c_1 \cdot \left(1 - e^{-c_2 s_{d4}}\right) - c_3 s_{d4}\right\} \\ \quad \cdot \left(M \cdot g \cdot \frac{a}{L} + M \cdot a_x \cdot \frac{h}{L}\right) \cdot R \end{cases} \tag{6}$$

It can be seen from Equation (6) that the driving torque of the ith wheel agent can be determined according to $\dot{\omega}_i$. Therefore, in this paper, $\dot{\omega}_i$ is regarded as the auxiliary control of the ith wheel agent, and the ideal torque satisfying the slip ratio tracking target can be obtained indirectly according to Equation (6).

D. THE TOPOLOGY DIAGRAM

The undirected digraph $G = (\Omega, \Pi, A)$ is said to contact the node set $\Omega = \{1, \ldots, N\}$, where N represents the number of nodes, $\Pi = \{(i, j), i, j \in \Omega\}$ represents the side set, and i and j can be called neighbors. The adjacency matrix is $A = [a_{ij}] \in R^{N\times N}$. The communication topology between the leader and the followers is denoted by a diagonal matrix $B = diag(b_1, b_2, \ldots, b_N), b_i > 0$.The in-degree matrix is

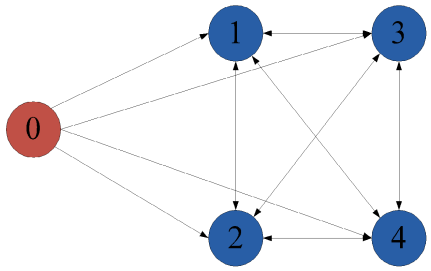

FIGURE 2. The communication topology of wheel agents system.

$D = diag(d_1, \ldots, d_N)$. The Laplacian matrix $L = [l_{ij}] \in R^{N\times N}$ is defined as $L = D - A$ with

$$l_{ij} = \begin{cases} -a_{ij}, & j \neq i \\ \sum_{j=1}^{N} a_{ij}, & j = i \end{cases} \tag{7}$$

According to the connection structure and internal working communication principle of distributed drive electric vehicles, the topological structure diagram of the ASR system based on graph theory is obtained, as shown in Fig. 3. The ideal slip rate is selected as the leader agent 0, and the four wheel subsystems are designated as the following agents 1, 2, 3 and 4. When designing the control strategy of a single driving wheel agent subsystem by considering the state information of its own agent and adjacent agent, it is understood that the actual slip rate of the system under different working conditions follows the optimal slip rate in finite time.

III. ADAPTIVE SLIDING MODE FAULT-TOLERANT CONTROL FOR AN ASR SYSTEM WITH ACTUATOR FAULTS

Define s_{d0} as the optimal slip ratio of the virtual leader:

$$s_{d0} = \frac{R\omega_0 - v_0}{R\omega_0} \tag{8}$$

where R, ω_0 and v_0 are the rolling radius of the wheel, the wheel angular velocity, and the longitudinal velocity of the virtual leader, respectively.

The goal of this paper is to design an adaptive sliding mode control protocol for a single driving wheel agent based on a MAS so that the actual slip rate of each wheel is able to track the optimal slippage infinite time under different road adhesion conditions. This approach can also avoid slippage when wheels are driving on different road surfaces, which improves the driving ability and directional stability of the electric vehicle during the driving process and improves the passing ability of the vehicle.

The error $\tilde{s}_{di}$ of the virtual leader's optimal slip ratio s_{d0} and the slip ratio of each wheel s_{di} is expressed as follows:

$$\tilde{s}_{di} = s_{di} - s_{do}$$

Then, differentiating equations (1) and (8), one obtains

$$\begin{aligned} \dot{s}_{di} &= \frac{(v_i + \Delta v_i)\dot{\omega}_i - (\dot{v}_i + \Delta\dot{v}_i)\omega_i + \Delta d_i}{R\omega_i^2} \\ &= f_i + z_i u_{ai} + d_i \end{aligned} \tag{9}$$

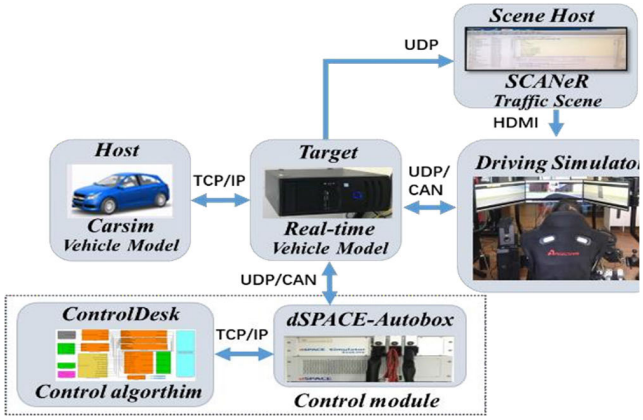

FIGURE 3. The structure of experimental platform.

where Δv_i and $\Delta\dot{v}_i$ are the unmodeled part of the ASR system and Δd_i is the external interference. $d_i = (\Delta v_i\dot{\omega}_i - \Delta\dot{v}_i\omega_i + \Delta d_i)/R\omega_i^2$, and $|d_i| < \bar{d}$, $\bar{d} > 0$. $u_0 = \dot{\omega}_0$ is the auxiliary control input of the virtual leader. $u_{ai} = \dot{\omega}_i$ is the auxiliary control input of the driving wheel agent. $z_0 = v_0/R\omega_0^2$, $z_i = v_i/R\omega_i^2$, $f_0 = -\dot{v}_0/R\omega_0$, $f_i = -\dot{v}_i/R\omega_i$.

Therefore, according to motion equation (4) and u_{ai} in (9), the driving torque T_{mi} of the ith wheel agent can be obtained.

We define the tracking errors of the slip rate as follows:

$$\begin{aligned} e_{1i} &= \sum_{j=1}^{N} l_{ij}\left(s_{di} - s_{dj}\right) + b_i\left(s_{di} - s_{d0}\right) \\ e_{2i} &= \sum_{j=1}^{N} l_{ij}\left(\dot{s}_{di} - \dot{s}_{dj}\right) + b_i\left(\dot{s}_{di} - \dot{s}_{d0}\right) \end{aligned} \tag{10}$$

Depending on where the electric vehicle failure occurs, faults can be classified into communication faults, equipment faults, sensor faults, and actuator faults. This paper focuses on the problem of actuator failure. If actuator faults occur in one or more of the four wheel agents in an electric vehicle, u_{ai} and u_i represent the actual auxiliary control and the designed auxiliary control of the i th wheel agent actuator, respectively. ξ_i and r_i represent the partial loss of effectiveness (PLOE) fault severity and the biased fault severity of the ith driving wheel agent, respectively. Then, the actual output of the actuator is described as follows:

$$u_{ai} = (1 - \xi_i)\, u_i + r_i \tag{11}$$

Assumption1. The PLOE fault severity and the biased fault severity of the ith wheel agent actuator are bounded. $0 < |\xi_i| \leq \bar{\xi} < 1$, and $|r_i| \leq \bar{r}$.

Define

$$\begin{aligned} &\tilde{s}_d = \left[\tilde{s}_{d1}, \tilde{s}_{d2}, \tilde{s}_{d3}, \tilde{s}_{d4}\right]^T, \dot{\tilde{s}}_d = \left[\dot{\tilde{s}}_{d1}, \dot{\tilde{s}}_{d2}, \dot{\tilde{s}}_{d3}, \dot{\tilde{s}}_{d4}\right]^T, \\ &x_{1i} = \int e_{1i}dt, \quad x_{2i} = e_{1i}, \quad \dot{\boldsymbol{X}}_{\boldsymbol{1}}, = [e_{11}, e_{12}, e_{13}, e_{14}]^T, \\ &\text{and } \dot{\boldsymbol{X}}_{\boldsymbol{2}} = [e_{21}, e_{22}, e_{23}, e_{24}]^T, \end{aligned}$$

then, $\dot{\boldsymbol{X}}_{\boldsymbol{1}} = (\boldsymbol{L}+\boldsymbol{B})\cdot\tilde{s}_d$ and $\dot{\boldsymbol{X}}_{\boldsymbol{2}} = (\boldsymbol{L}+\boldsymbol{B})\cdot\dot{\tilde{s}}_d$. The ideal slip rate tracking error equation of the ASR system can be written as follows:

$$\begin{aligned}\dot{\boldsymbol{X}}_1 &= \boldsymbol{X}_2\\ \dot{\boldsymbol{X}}_2 &= (\boldsymbol{L}+\boldsymbol{B})\cdot(\boldsymbol{F}_i-\boldsymbol{F}_{\boldsymbol{0}}-\boldsymbol{Z}_{\boldsymbol{0}}u_0+(\boldsymbol{I}_{\boldsymbol{n}}-\boldsymbol{\xi})\boldsymbol{Z}_d\boldsymbol{U}+\boldsymbol{D}+\boldsymbol{R})\end{aligned} \tag{12}$$

where

$$\begin{aligned}&\boldsymbol{F}_{\boldsymbol{0}} = 1_N\otimes f_0,\ \ \boldsymbol{F}_i = [f_1,f_2,f_3,f_4]^T, \boldsymbol{Z}_d = diag(z_1,\ldots,z_4),\\ &\boldsymbol{Z}_0 = 1_N\otimes z_0, \boldsymbol{\xi} = diag(\xi_1,\ldots\xi_4), \boldsymbol{D} = [d_1,\ldots,d_4]^T\\ &\boldsymbol{R} = [r_1,\ldots,r_4]^T,\ \ \boldsymbol{U} = [u_1,u_2,u_3,u_4]^T,\\ &\boldsymbol{X}_1 = [x_{11},x_{12},x_{13},x_{14}]^T,\ \text{ and }\ \boldsymbol{X}_2 = [x_{21},x_{22},x_{23},x_{24}]^T.\end{aligned}$$

A. THE NONSINGULAR TERMINAL SLIDING MODE CONTROL FOR THE ASR SYSTEM WITH AN ADAPTIVE ESTIMATION MECHANISM CONTROLLER SWITCHING ITEM

According to equation (11), when $\xi_i = 0$ and $r_i = 0$, there is no actuator fault, or the fault has been repaired. A NTSM controller for a single driving wheel agent is designed to make the actual slip rate track the ideal slip rate for the ASR system in finite time.

The NTSM manifold is designated as

$$s_i = x_{1i} + \frac{1}{\varepsilon}x_{2i}^{\frac{p}{q}},\quad i = 1,2,3,4 \tag{13}$$

where $\varepsilon > 0$, and p and q (where $p > q > 0$) are positive odd numbers. Then, the nonsingular terminal sliding manifold matrix form of the ASR system is as follows:

$$\boldsymbol{S} = \boldsymbol{X}_1 + \frac{1}{\varepsilon}\boldsymbol{X}_2^{\frac{p}{q}} \tag{14}$$

where $\boldsymbol{S} = [s_1,s_2,s_3,s_4]^T$ and $\boldsymbol{X}_2^{p/q} = [x_{21}^{p/q},x_{22}^{p/q},x_{23}^{p/q},x_{24}^{p/q}]^T$.

It is thus concluded that the control protocol is as follows:

$$u_i = u_{i\_eq} + u_{i\_s} \tag{15}$$

$$\begin{aligned}u_{i\_eq} &= \frac{R\omega_i^2}{v_i}(l_{ii}+b_i)^{-1}\left[-\sum_{j\neq i}^{l_{ij}u_j} -\frac{q}{p}\varepsilon x_{2i}^{2-\frac{p}{q}}\right]\\ &\quad+\frac{R\omega_i^2}{v_i}\left[f_0-f_i+\frac{v_0}{R\omega_0}u_0\right]\\ u_{i\_s} &= -\frac{R\omega_i^2}{v_i}(l_{ii}+b_i)^{-1}(-\beta_i\,\mathrm{sgn}(s_i)-\gamma_i s_i)\end{aligned} \tag{16}$$

where $\beta_i > 0$ and $\gamma_i > 0$.

The upper bound $\bar{d}$ of uncertainty in the ASR system, which can include actual physical system damping, plant parameter variations, externally loaded disturbances, and unmolded and nonlinear dynamics, is difficult to obtain because of the variable driving cycle and the cooperative work of multiple actuators. If the gain of the sliding mode switching term is overestimated, controller chattering and high energy consumption will occur.

Therefore, this paper proposes an adaptive estimation mechanism of controller switching item gain as follows:

$$\dot{\hat{\beta}}_i = \rho\frac{p}{q}\frac{1}{\varepsilon}x_{2i}^{\frac{p}{q}-1}|s_i| \tag{17}$$

where $\hat{\beta}_i$ is the estimated value for the controller (16) switching item gain β_i.

Control protocol u_{i_s} is modified as follows:

$$u_{i\_s} = -\frac{R\omega_i^2}{v_i}(l_{ii}+b_i)^{-1}\left(-\hat{\beta}_i\,\mathrm{sgn}(s_i)-\gamma_i s_i\right) \tag{18}$$

Therefore, the matrix form of the control input is as follows:

$$\begin{aligned}\boldsymbol{U} = \boldsymbol{Z}_d^{-1}(\boldsymbol{L}+\boldsymbol{B})^{-1}\cdot\left[\hat{\boldsymbol{h}}(\boldsymbol{s})-\frac{q}{p}\varepsilon\boldsymbol{X}_2^{2-\frac{p}{q}}\right]\\ +\boldsymbol{Z}_d^{-1}(\boldsymbol{F}_0-\boldsymbol{F}_i+\boldsymbol{Z}_0u_0)\end{aligned} \tag{19}$$

where $\hat{\boldsymbol{h}}(\boldsymbol{S}) = -[\hat{\beta}_1\ \mathrm{sgn}(s_1)+\gamma_1 s_1, \hat{\beta}_2\mathrm{sgn}(s_2)+\gamma_2 s_2, \hat{\beta}_3\ \mathrm{sgn}(s_3)+\gamma_3 s_3, \hat{\beta}_4\ \mathrm{sgn}(s_4)+\gamma_4 s_4]^T$.

Theorem 1. For an ASR system without actuator faults, if the NTSM manifolds are chosen as (13), the control input u_i is designated as (15), and the adaptive estimation mechanism controller switching item gain $\hat{\beta}_i$ is designated as (17), then the ASR system (12) can be guaranteed to be stable at the equilibrium point in finite time.

Proof. Consider the following Lyapunov function:

$$V = \frac{1}{2}\boldsymbol{S}^T\boldsymbol{S} + \frac{1}{2\rho}\sum_{i=1}^{4}(\beta_i-\hat{\beta}_i)^2$$

where ρ is the designed parameter, and $\rho > 0$.

Differentiating V with respect to time yields:

$$\begin{aligned}\dot{V} &= \boldsymbol{S}^T\dot{\boldsymbol{S}} - \frac{1}{\rho}\sum_{i=1}^{4}(\beta_i-\hat{\beta}_i)\dot{\hat{\beta}}_i\\ \dot{V} &= \boldsymbol{S}^T\{\frac{p}{q}\frac{1}{\varepsilon}\,\mathrm{diag}\,(\boldsymbol{X}_2^{\frac{p}{q}-1})[\frac{q}{p}\varepsilon\boldsymbol{X}_2^{2-\frac{p}{q}}+(\boldsymbol{L}+\boldsymbol{B})\\ &\quad(\boldsymbol{F}_i-\boldsymbol{F}_{\boldsymbol{0}}-\boldsymbol{Z}_{\boldsymbol{0}}\boldsymbol{U}_0+(\boldsymbol{L}+\boldsymbol{B})^{-1}(\boldsymbol{h}(\boldsymbol{S})-\frac{q}{p}\varepsilon\boldsymbol{X}_2^{2-\frac{p}{q}})\\ &\quad+\boldsymbol{Z}_0u_0+\boldsymbol{F}_0-\boldsymbol{F}_i)+\boldsymbol{D})]\}\end{aligned} \tag{20}$$

Then, substituting the control protocol (15) into (20), the following can be obtained:

$$\begin{aligned}\dot{V} = \boldsymbol{S}^T[\frac{p}{q}\frac{1}{\varepsilon}\,\mathrm{diag}(\boldsymbol{X}_2^{\frac{p}{q}-1})((\boldsymbol{L}+\boldsymbol{B})\boldsymbol{D}+\hat{\boldsymbol{h}}(\boldsymbol{S}))]\\ -\frac{1}{\rho}\sum_{i=1}^{4}(\beta_i-\hat{\beta}_i)\dot{\hat{\beta}}_i\end{aligned}$$

Then, the switching gain for the sliding mode control protocol is selectas $\boldsymbol{\beta} = (\boldsymbol{L}+\boldsymbol{B})\boldsymbol{D}$.

$$\dot{V} = \sum_{i=1}^{4}s_i\frac{p}{q\varepsilon}x_{2i}^{\frac{p}{q}-1}[\beta_i-\hat{\beta}_i\,\mathrm{sgn}(s_i)] - \boldsymbol{S}^T\frac{p}{q\varepsilon}\,\mathrm{diag}(\boldsymbol{X}_2^{\frac{p}{q}-1})\boldsymbol{\gamma}\boldsymbol{S}$$

$$
\begin{aligned}
&-\frac{1}{\rho}\sum_{i=1}^{4}(\beta_i-\hat{\beta}_i)\dot{\hat{\beta}}_i \\
&\le \sum_{i=1}^{4}\frac{p}{q}\frac{1}{\varepsilon}x_{2i}^{\frac{p}{q}-1}(\beta_i-\hat{\beta}_i)\,|s_i| - \boldsymbol{S}^T\frac{p}{q}\frac{1}{\varepsilon}\ \mathrm{diag}(\boldsymbol{X}_2^{\frac{p}{q}-1})\boldsymbol{\gamma}\boldsymbol{S} \\
&\quad -\frac{1}{\rho}\sum_{i=1}^{4}(\beta_i-\hat{\beta}_i)\dot{\hat{\beta}}_i \\
&= \sum_{i=1}^{4}(\beta_i-\hat{\beta}_i)\left[\frac{p}{q}\frac{1}{\varepsilon}x_{2i}^{\frac{p}{q}-1}\,|s_i| - \frac{1}{\rho}\dot{\hat{\beta}}_i\right] \\
&\quad -\boldsymbol{S}^T\frac{p}{q}\frac{1}{\varepsilon}\ \mathrm{diag}(X_2^{\frac{p}{q}-1})\boldsymbol{\gamma}\boldsymbol{S} \qquad (21)
\end{aligned}
$$

Then, substituting equation (17) into equation (21), we obtain

$$
\dot{V} \le -\boldsymbol{S}^T\frac{p}{q\varepsilon}\ \mathrm{diag}(\boldsymbol{X}_2^{\frac{p}{q}-1})\boldsymbol{\gamma}\boldsymbol{S} \le -\frac{p}{q\varepsilon}\lambda_{\min}(\mathrm{diag}(\boldsymbol{X}_2^{\frac{p}{q}-1})\boldsymbol{\gamma})\,\|\boldsymbol{S}\|^2 \le 0 \qquad (22)
$$

According to the Lyapunov stability theorem, $\boldsymbol{S}=0$ and $\dot{\boldsymbol{S}}=0$ can be obtained. According to equation (13), $\boldsymbol{e}_{1i}=0$, $\boldsymbol{e}_{2i}=0$ and $s_{di}=s_{dj}=s_{d0}$. The actual slip rate of each driving wheel agent can follow the ideal slip rate within a finite time to avoid drive slippage of the wheels on the road.

After reaching the sliding surface, one can obtain $\boldsymbol{S}=0$. According to (22), $\lim_{t\to t_s} V(t)=0$. The time for the system state to reach the sliding manifold is

$$
t_v \le \ln(V(0))/[\frac{2p}{q\varepsilon}\lambda_{\min}(\mathrm{diag}(\boldsymbol{X}_2^{\frac{p}{q}-1})\,(\boldsymbol{L}+\boldsymbol{B})\cdot\boldsymbol{\gamma})]
$$

The system state on the sliding surface satisfies $\boldsymbol{S}=0$. According to (14), the time for the system state to go from the initial state on the sliding surface to the origin is:

$$
t_s = \frac{p}{\varepsilon(p-q)}\,|X_1(0)|^{(p-q)/p} \qquad (23)
$$

Therefore, the finite time when the actual slip rate reaches the ideal slip rate is $t_1 \le t_v + t_s$.

B. ADAPTIVE NONSINGULAR RTERMINAL SLIDING MODE FAULT-TOLERANT CONTROL FOR AN ASR SYSTEM WITH ACTUATOR FAULTS

The ASR system of the four driving wheel agents of the distributed drive electric vehicle is equipped with independent driving actuators, which can independently control the driving force of each wheel according to the change in the road friction coefficient.

For the fault of each driving wheel agent in the ASR system (when $\xi_i \neq 0$ and $r_i \neq 0$), an adaptive NTSM control protocol based on multiple agents is proposed in this paper to achieve fast tracking of the optimal slip ratio in the event of actuator failure.

Here,

$$
\mathrm{diag}(\boldsymbol{\sigma}) = \mathrm{diag}(\boldsymbol{I}_n) - (L+B)\mathrm{diag}(\boldsymbol{\xi})(L+B)^{-1} \qquad (24)
$$

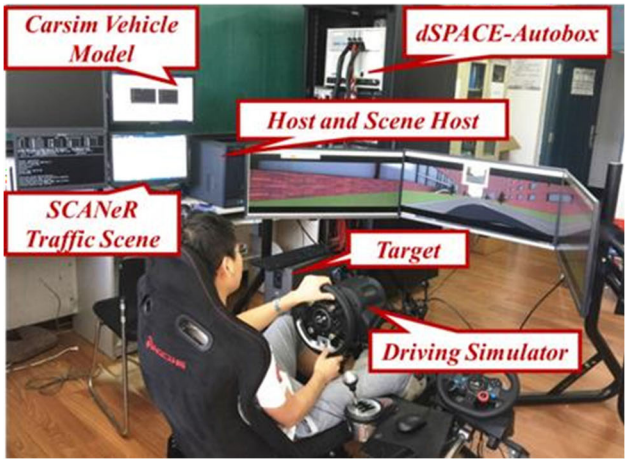

FIGURE 4. The experimental platform.

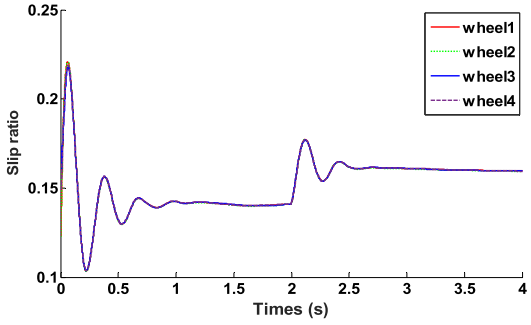

FIGURE 5. The slip ratio with the NTSM control.

where $\boldsymbol{\sigma}=[\sigma_1,\sigma_2,\sigma_3,\sigma_4]^T$, $\sigma_i>0$, and $i=1,2,3,4$.

Theorem 2. For an ASR system with actuator faults (12), if the NTSM manifolds are chosen as (13), the control input u_i is designated as (15), and the adaptive estimation mechanism of the controller switching item gain $\dot{\hat{\beta}}_i$(17) and the design parameter σ_i(24) are designated, then the ASR system (12) can be guaranteed to be stable at the equilibrium point in finite time.

Proof. Consider the following Lyapunov function:

$$
V = \frac{1}{2}\boldsymbol{S}^T\boldsymbol{S} + \frac{1}{2\rho}\sum_{i=1}^{4}\sigma_i(\beta_i-\hat{\beta}_i)^2 \qquad (25)
$$

$$
\begin{aligned}
\dot{V} = \boldsymbol{S}^T[&\frac{p}{q}\frac{1}{\varepsilon}\mathrm{diag}(\boldsymbol{X}_2^{\frac{p}{q}-1})((\boldsymbol{L}+\boldsymbol{B}) \\
&(\boldsymbol{F}_i-\boldsymbol{F_0}-\boldsymbol{Z_0U}_0+\boldsymbol{Z}_d\boldsymbol{U}+\boldsymbol{D}+\boldsymbol{R}) - (\boldsymbol{L}+\boldsymbol{B})\mathrm{diag}(\boldsymbol{\xi}) \\
&\boldsymbol{Z}_d\boldsymbol{U}+\frac{q}{p}\varepsilon\boldsymbol{X}_2^{2-\frac{p}{q}})] - \frac{1}{\rho}\sum_{i=1}^{4}\sigma_i(\beta_i-\hat{\beta}_i)\dot{\hat{\beta}}_i \qquad (26)
\end{aligned}
$$

Then, substituting (19) into (26), one obtains

$$
\begin{aligned}
\dot{V} = \boldsymbol{S}^T[&\frac{p}{q}\frac{1}{\varepsilon}\mathrm{diag}(\boldsymbol{X}_2^{\frac{p}{q}-1})((\boldsymbol{L}+\boldsymbol{B})(\boldsymbol{D}+\boldsymbol{R})+\boldsymbol{h}(\boldsymbol{S}) \\
&-(\boldsymbol{L}+\boldsymbol{B})\mathrm{diag}(\boldsymbol{\xi})\cdot((\boldsymbol{L}+\boldsymbol{B})^{-1}(\boldsymbol{h}(\boldsymbol{S})-\frac{q}{p}\varepsilon\boldsymbol{X}_2^{2-\frac{p}{q}})
\end{aligned}
$$

$$+\boldsymbol{F}_0-\boldsymbol{F}_i+\boldsymbol{Z}_0u_0))]-\frac{1}{\rho}\sum_{i=1}^{4}\sigma_i(\beta_i-\hat{\beta}_i)\dot{\hat{\beta}}_i \quad (27)$$

Define

$$\boldsymbol{\psi}=\mathrm{diag}\boldsymbol{\xi})[(\boldsymbol{L}+\boldsymbol{B})^{-1}\frac{q}{p}\varepsilon\boldsymbol{X}_2^{\frac{p}{q}-1}-\boldsymbol{F}_0+\boldsymbol{F}_i-\boldsymbol{Z}_0u_0] \quad (28)$$

Then,

$$\begin{aligned}\dot{V}=&\boldsymbol{S}^T[\frac{p}{q}\frac{1}{\varepsilon}\mathrm{diag}(\boldsymbol{X}_2^{\frac{p}{q}-1})((\boldsymbol{L}+\boldsymbol{B})(\boldsymbol{D}+\boldsymbol{R}+\boldsymbol{\psi})\\&+(\mathrm{diag}(\boldsymbol{I}_n)-(\boldsymbol{L}+\boldsymbol{B})\cdot\mathrm{diag}(\boldsymbol{\xi})(\boldsymbol{L}+\boldsymbol{B})^{-1})\boldsymbol{h}(\boldsymbol{S}))]\\&-\frac{1}{\rho}\sum_{i=1}^{4}\sigma_i(\beta_i-\hat{\beta}_i)\dot{\hat{\beta}}_i\end{aligned} \quad (29)$$

The parameters $\boldsymbol{\psi}$ and $\boldsymbol{\beta}$ are designated satisfy the following equation:

$$\mathrm{diag}(\boldsymbol{\sigma})\cdot\boldsymbol{\beta}=(\boldsymbol{L}+\boldsymbol{B})(\boldsymbol{D}+\boldsymbol{R}-\boldsymbol{\psi}) \quad (30)$$

Then,

$$\begin{aligned}\dot{V}=&\boldsymbol{S}^T\frac{p}{q}\frac{1}{\varepsilon}\mathrm{diag}(\boldsymbol{X}_2^{\frac{p}{q}-1})\mathrm{diag}(\boldsymbol{\sigma})(\boldsymbol{\beta}-\hat{\boldsymbol{\beta}}\mathrm{sgn}(\boldsymbol{S}))\\&-\boldsymbol{S}^T\frac{p}{q}\frac{1}{\varepsilon}\mathrm{diag}(\boldsymbol{X}_2^{\frac{p}{q}-1})\mathrm{diag}(\boldsymbol{\sigma})\boldsymbol{\gamma}\boldsymbol{S}-\frac{1}{\rho}\sum_{i=1}^{4}\sigma_i(\beta_i-\hat{\beta}_i)\dot{\hat{\beta}}_i\\&=-\boldsymbol{S}^T\frac{p}{q}\frac{1}{\varepsilon}\mathrm{diag}(\boldsymbol{X}_2^{\frac{p}{q}-1})\mathrm{diag}(\boldsymbol{\sigma})\boldsymbol{\gamma}\boldsymbol{S}\\&+\sum_{i=1}^{4}s_i\frac{p}{q\varepsilon}x_{2i}^{\frac{p}{q}-1}\sigma_i[\beta_i-\hat{\beta}_i\mathrm{sgn}(s_i)]\\&-\frac{1}{\rho}\sum_{i=1}^{4}\sigma_i(\beta_i-\hat{\beta}_i)\dot{\hat{\beta}}_i\le-\boldsymbol{S}^T\frac{p}{q}\frac{1}{\varepsilon}\mathrm{diag}(\boldsymbol{X}_2^{\frac{p}{q}-1})\\&+\mathrm{diag}(\boldsymbol{\sigma})\boldsymbol{\gamma}\boldsymbol{S}\sum_{i=1}^{4}\frac{p}{q\varepsilon}x_{2i}^{\frac{p}{q}-1}\sigma_i[\beta_i-\hat{\beta}_i]\,|s_i|\\&-\frac{1}{\rho}\sum_{i=1}^{4}\sigma_i(\beta_i-\hat{\beta}_i)\dot{\hat{\beta}}_i\\&\le-\boldsymbol{S}^T\frac{p}{q}\frac{1}{\varepsilon}\mathrm{diag}(\boldsymbol{X}_2^{\frac{p}{q}-1})\mathrm{diag}(\boldsymbol{\sigma})\boldsymbol{\gamma}\boldsymbol{S}\\&+\sum_{i=1}^{4}\sigma_i[\beta_i-\hat{\beta}_i](\frac{p}{q\varepsilon}x_{2i}^{\frac{p}{q}-1}|s_i|-\frac{1}{\rho}\dot{\hat{\beta}}_i)\\&\le-\frac{2p}{q\varepsilon}\lambda_{\min}(\mathrm{diag}(\boldsymbol{X}_2^{\frac{p}{q}-1})\cdot\mathrm{diag}(\boldsymbol{\sigma})\cdot\boldsymbol{\gamma})V\le0\end{aligned} \quad (31)$$

According to the Lyapunov stability theorem, the control protocol (15) and the switching gain (17) proposed in this paper can ensure the actual slip ratio of each driving wheel agent to track the optimal slip ratio in a finite time window when actuator faults occur.

According to (31) and (14), the finite time is:

$$t_2\le\ln(V(0))/[\frac{2p}{q\varepsilon}\lambda_{\min}(\mathrm{diag}(\boldsymbol{X}_2^{\frac{p}{q}-1})\cdot\mathrm{diag}(\boldsymbol{\sigma})\cdot\boldsymbol{\gamma})]+t_s \quad (32)$$

According to the motion equation, by substituting (15) into (4), the driving torque of the ith wheel can be obtained as follows:

$$\begin{aligned}T_{mi}=I\{&\frac{R\omega_i^2}{v_i}(l_{ii}+b_i)^{-1}[-\sum_{j\ne i}^{l_{ij}u_j}-\frac{q}{p}\varepsilon x_{2i}^{2-\frac{p}{q}}-\hat{\beta}_i\,\mathrm{sgn}\,(s_i)\\&-\gamma_i s_i]+\frac{R\omega_i^2}{v_i}[f_0-f_i+\frac{v_0}{R\omega_0}u_0]\}+F_{xi}R\end{aligned}$$

The driving torque is adjusted by a sliding mode control strategy to change the force of the driving wheel and achieve the control goal in this paper.

IV. SIMULATION AND ANALYSIS

The experimental platform includes a driving simulator, a dSPACE for running control algorithms, a host for running Carsim vehicle model and SCANeR traffic scene model, and a target machine for running real-time vehicle model. Driver to manipulate the steering wheel and pedals in a driving simulator to produce the steering wheel Angle and the drive pedal signal, after CAN turn Ethernet module to the target, the demand of real-time vehicle model is used to calculate for the total torque, the real-time slip ratio and the current pavement of optimal slip ratio, through the Ethernet switch CAN module is sent to the ASR Autobox control module, get four wheel torque control signal and sent to the target machine, the calculation to obtain the vehicle's position changes, from Ethernet to host traffic scene, vehicle attitude change of traffic scene, the driver according to the change of scene to control the vehicle. Then a closed loop is formed. The structure of experimental platform is shown in Fig.3. The experimental platform is shown in Fig.4

According to the connection structure shown in Fig. 2, the adjacency matrix $\boldsymbol{A}$, the in-degree matrix $\boldsymbol{D}$ and the matrix $\boldsymbol{B}$ are as follows:

$$\begin{aligned}A=&\begin{bmatrix}0&1&1&1\\1&0&1&1\\1&1&0&1\\1&1&1&0\end{bmatrix}\boldsymbol{D}=\begin{bmatrix}4&0&0&0\\0&4&0&0\\0&0&4&0\\0&0&0&4\end{bmatrix}\\\boldsymbol{B}=&\begin{bmatrix}1&0&0&0\\0&1&0&0\\0&0&1&0\\0&0&0&1\end{bmatrix}\end{aligned} \quad (33)$$

Then, the Laplacian matrix $\boldsymbol{L}$ is as follows:

$$\boldsymbol{L}=\boldsymbol{D}-\boldsymbol{A}=\begin{bmatrix}4&-1&-1&-1\\-1&4&-1&-1\\-1&-1&4&-1\\-1&-1&-1&4\end{bmatrix} \quad (34)$$

We designate the initial speed of all four wheels as $v_0=2.4m/s$, with design parameters $\gamma_i=10$ and $\rho=10$. We assume that the initial values of the slip ratios of the four wheel agents are 0.12, 0.1, 0.15 and 0.17. The sliding manifold is designated as $s_i=x_{1i}+10^{-1}x_{2i}^{5/3}$. We assume that

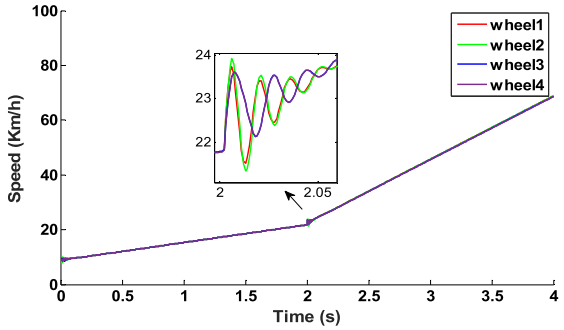

FIGURE 6. The speed with the NTSM control.

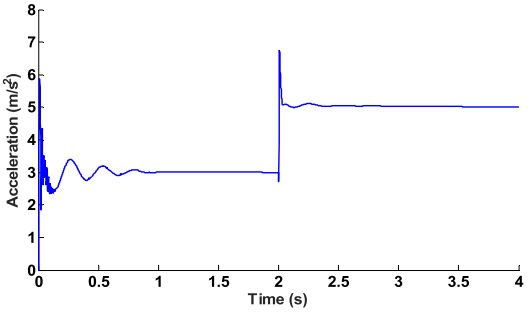

FIGURE 7. The acceleration with the NTSM control.

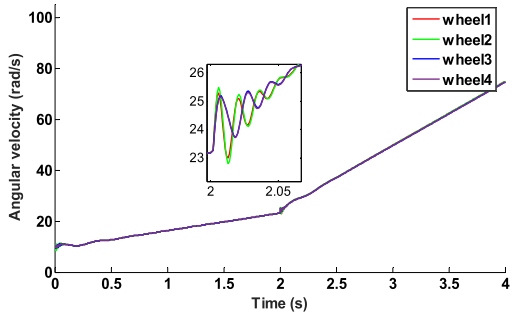

FIGURE 8. The angular velocity with the NTSM control.

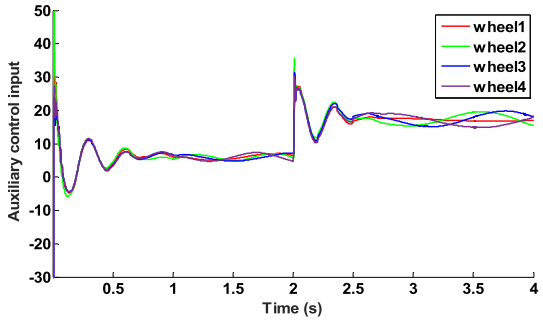

FIGURE 9. The auxiliary control with the NTSM control.

the disturbances are $d_1 = 0.5\sin(20t)$, $d_2 = 0.5\sin(20t + 0.25)$, $d_3 = 0.6\sin(20t + 0.5)$, and $d_4 = 0.7\sin(20t + 0.75)$.

The parameters of the vehicle are as follows:

APD16 motor made by the Protean Electric Company is selected, and the parameters of the PD16 motor are listed in Table 2.

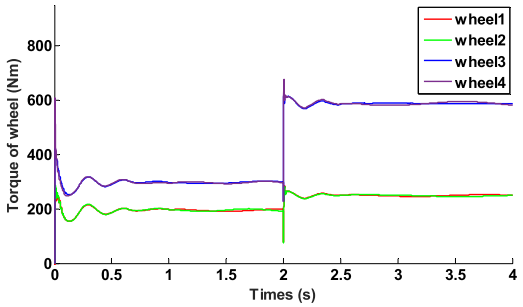

FIGURE 10. The torque of wheel with the NTSM control.

TABLE 1. The parameters of the vehicle.

Project	Numerical
Overall vehicle mass	1100 kg
Sprung mass	980 kg
Effective rolling radius of tire	304 mm
Unloaded (free) radius	310.8 mm
Roll inertia of tire	$2.88\,\mathrm{kg}\cdot\mathrm{m}^2$
Length of axial	2600 mm
Length of front axle	1040 mm
Length of rear axle	1560 mm
Height of centroid	540 mm

TABLE 2. The parameters of the PD16 motor.

Parameter	Numerical value
Peak Output Power	45kW
Continuous Output Power	33kW
Peak Torque	800Nm
Continuous Torque	450Nm
Maximum Speed	1350rpm

TABLE 3. The optimal slip ratio and adhesion coefficient of differents pavements.

Load surface	c_1	c_2	c_3	s_{d0}	$\mu_{\max}$
Wet cobblestone	0.4004	33.708	0.120	0.14	0.34
Dry cement	1.1973	25.168	0.53733	0.16	1.09

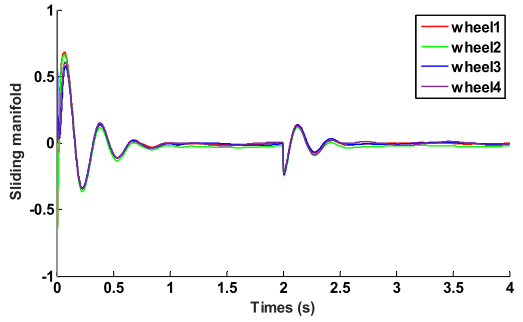

FIGURE 11. The sliding manifold with the adaptive NTSM control.

The Optimal slip ratio of different pavements and adhesion coefficient are listed in TABLE 3.

A. THE NONSINGULARTERMINAL SLIDING MODE CONTROL

The simulation time is 4 s, and the road conditions are set as wet cobblestone for 0-2 s and dry cement for 2-4 s. The

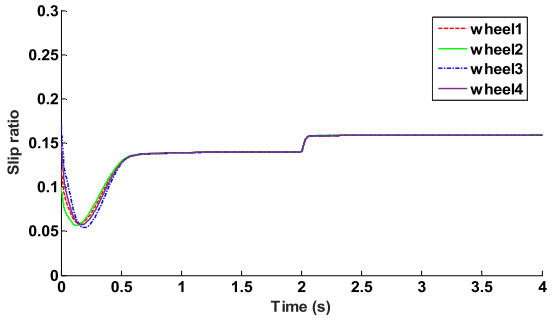

FIGURE 12. The slip ratio with the adaptive NTSM control.

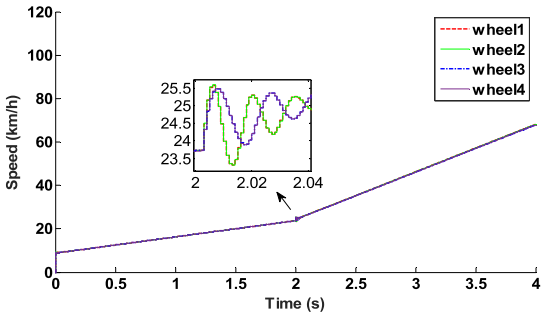

FIGURE 13. The speed with the adaptive NTSM control.

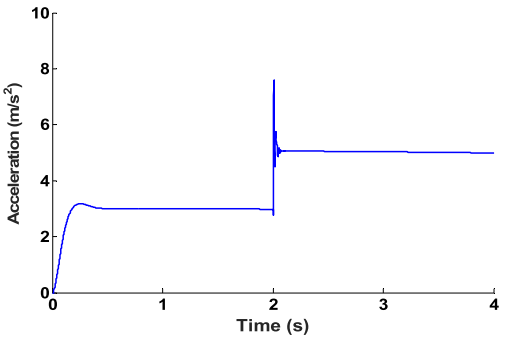

FIGURE 14. The acceleration with the adaptive NTSM control.

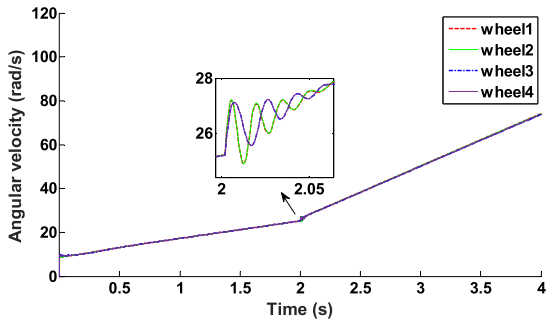

FIGURE 15. The angular velocity with the adaptive NTSM control.

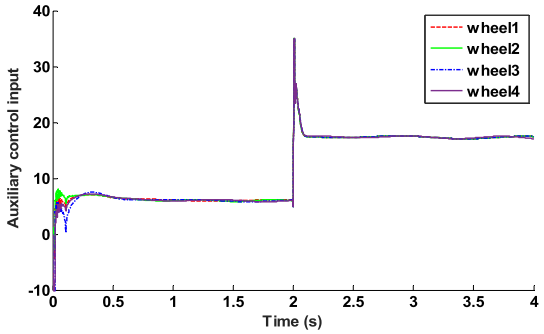

FIGURE 16. The auxiliary control with the adaptive NTSM control.

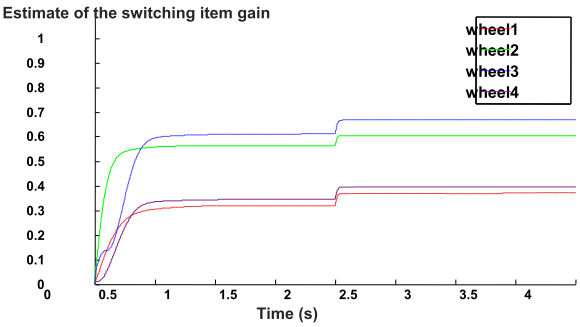

FIGURE 17. Estimate of switching item gain.

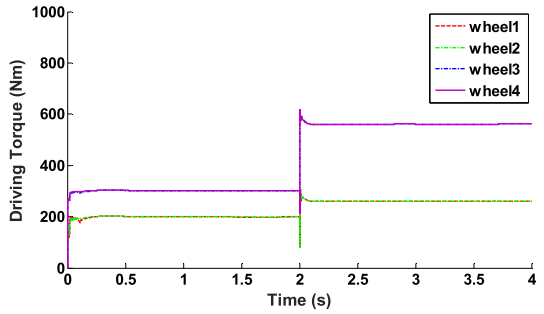

FIGURE 18. The driving torque with the adaptive NTSM control.

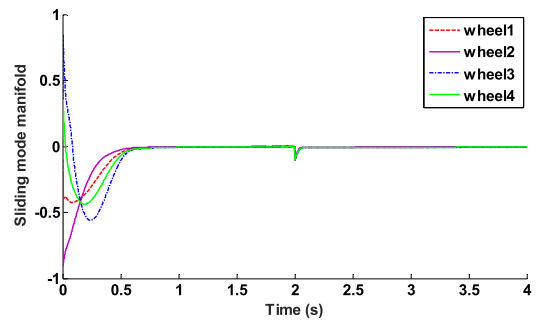

FIGURE 19. The sliding mode manifold with the adaptive NTSM control.

pavement parameter setting can be completed in Carsim. Lagrange interpolation method was used to estimate the peak adhesion coefficient and the optimal slip ratio of the current road surface [41]. In the table 3, the optimal slip ratios are $\lambda_{d0} = 0.14$ and $\lambda_{d0} = 0.16$ respectively. The parameters are $\xi_i = 0$ and $r_i = 0$. Under the unmodeled part of system and the external interference unknown conditions, the NTSM control(15), (16), the gain of switching terms are set to be $\beta_i = 5$, and the adaptive NTSM control (15), (18) with the adaptive mechanism (17) are adopted respectively, to carry out simulation experiment analysis. The simulation is shown in Fig.5-11 and Fig.12-19 respectively. As shown in Fig.4 and

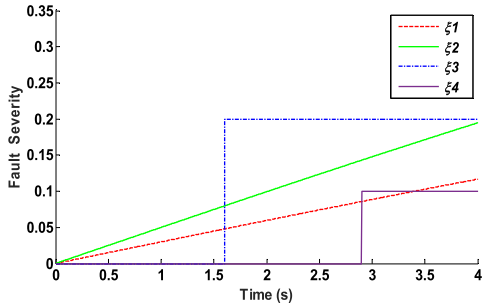

FIGURE 20. Fault severity.

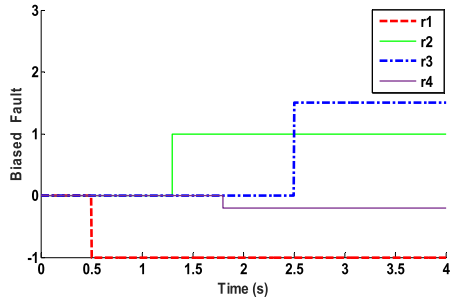

FIGURE 21. Biased fault.

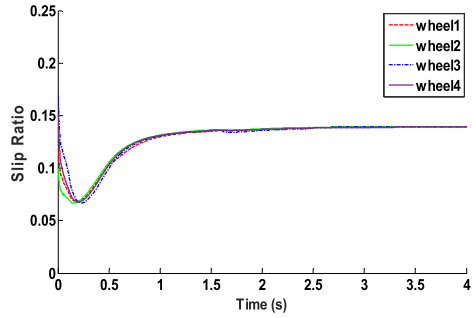

FIGURE 22. The slip ratio with fault-tolerant control.

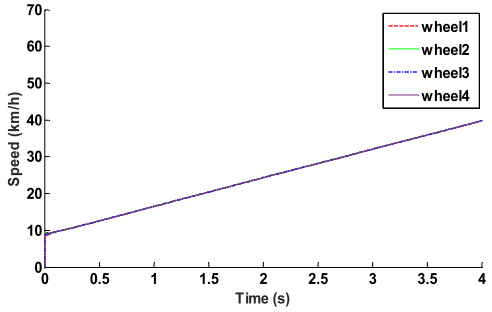

FIGURE 23. The speed with fault-tolerant control.

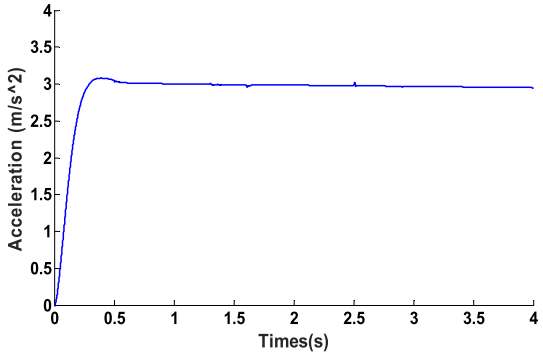

FIGURE 24. Longitudinal acceleration.

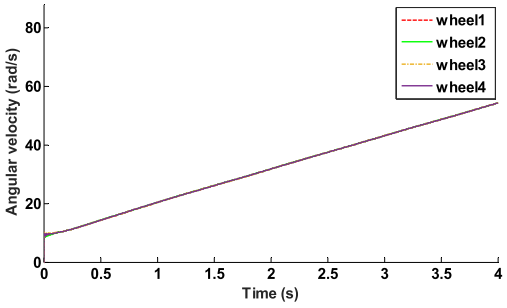

FIGURE 25. The angular velocity with fault-tolerant control.

Fig 11, as for known upper bound interference and unknown interference under joint road conditions, the slip ratio of the four wheel agents can reach the ideal slip ratio quickly. Compared with the convergence time of the four wheel slip ratios under the adaptive NTSM control strategy in Fig.12, the convergence time in Fig.5 is twice as long as the latter. The longitudinal speed and the angular velocity of the wheel and the longitudinal acceleration of the vehicle are shown in Fig.6-8 and Fig.13-15. Also the longitudinal acceleration of $a = 5m/s^2$ is achieved in the same convergence time of each controller in Fig.7 and Fig.14, it can be conclude that two control methods can stabilize the longitudinal acceleration rapidly in the same convergence time of each other. After the road surface switching, the system can quickly reach the stable state under the condition of interference change. After 2s of road switching, the longitudinal speed of the wheel increases from 24 to 66 km/h under the adaptive NTSM control in Fig.12, and the acceleration performance is good. Compared with the Fig.7, the acceleration performance is better than the NTSM tracking control with the constant switching gain. The method proposed in this paper can prevent excessive driving wheel slippage under the road switching, and the vehicle driving performance is basically unchanged when the system stability is satisfied. And it can be seen that using the adaptive mechanism for the gain of the switching term in the NTSM controller can significantly improve the convergence rate.

The control input signals of the two controllers are shown in Fig.9 and Fig.16. The driving torque is shown in Fig.10 and Fig.18.Compared with the Fig.9 and Fig.10, it can be seen that chattering was significantly reduced in Fig. 16and Fig.18, so that pulses of the torque are reduced effectively. In addition, the control inputs and the torque of wheel tend to stable state quickly in finite time. The adaptive estimation of the switching gain for the controller shown in Fig.17 effectively compensates for the influence of disturbance and road surface switching on the system stability and driving performance, and the overestimation of the unknown is prevented.

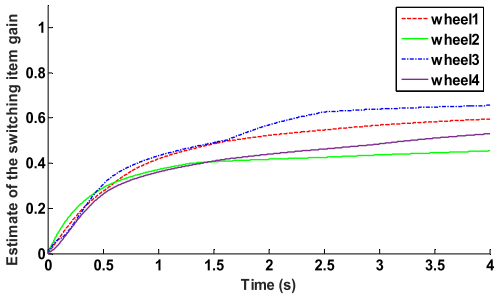

FIGURE 26. The estimate of switching item gain with fault-tolerant control.

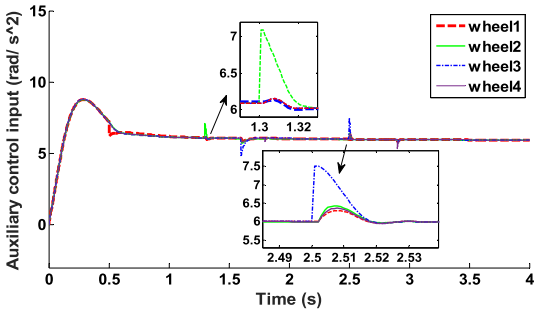

FIGURE 27. The auxiliary control with fault-tolerant control.

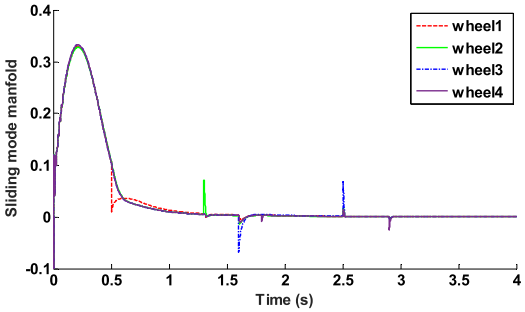

FIGURE 28. The sliding mode manifold with fault-tolerant control.

The NTSM manifold is shown in Fig.11 and Fig.19. The system state reaches the sliding mode manifold rapidly from the initial value, so that the actual slip ratio reaches the optimal slip ratio in Fig.5 and Fig.12. Compared with the NTSM controller, *i*th as the better universal applicability. The experimental results show that the adaptive NTSM controller can rapidly adjust the driving torque to obtain greater adhesion under different road conditions than the NTSM controller, the safety and robustness of the system are improved effectively, and the acceleration performance is guaranteed. At the same time it has addressed the overestimation problem of the switching gain and reduced the loss of energy.

B. ADAPTIVE NONSINGULARTERMINALSLIDING MODE FAULT-TOLERANT CONTROL

The road condition is set as wet cobblestone for 0-4s. The simulation parameters are the same as those in section 4.1. The actuator faults ξ_i and r_i are shown in Fig.20 and Fig.21. The vehicle starts accelerating at initial velocity on the wet

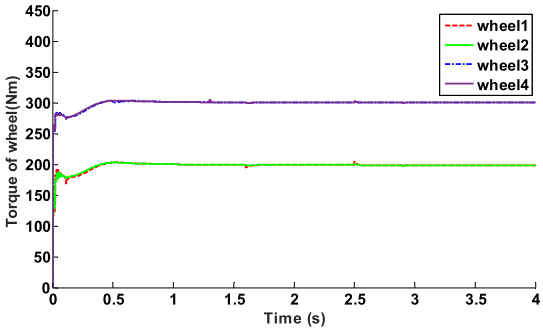

FIGURE 29. The driving torque with fault-tolerant control.

cobblestone. It can be seen in Fig.21 that the actual slip ratio of each driving wheel agent tracks the optimal slip ratio within 1s when the actuator faults occur. The longitudinal speed, the angular velocity of the wheel and the longitudinal acceleration of the vehicle are shown in Fig.23, Fig.24 and Fig.25. The proposed method does not change the vehicle dynamic performance under actuator faults while preventing wheel slippage. An adaptive estimation mechanism of the control switch gain is used in Fig. 26 to avoid the gain overestimation problem and excessive controller energy consumption. The control input and the NTSM manifold are shown in Fig. 27 and Fig. 28. The system state rapidly reaches the sliding mode manifold, and there is no obvious buffeting phenomenon in the sliding mode control under actuator faults. The required torques of the front wheels and the rear wheels are shown in Fig.29. The Simulink and CarSim cosimulation results show that the proposed method improves the fault tolerance and robustness. This approach can realize the actual slip ratio and track the optimal slip rate in a finite time under different road adhesion conditions.

V. CONCLUSION

To improve the robustness, adaptability, and fault tolerance and reduce the computational complexity of an ASR system of a distributed drive electric vehicle, a NTSM fault-tolerant control method based on multi-agent theory is proposed in this paper. Based on graph theory, a cooperation model of each driving wheel agent subsystem is established. According to the state information of the agent subsystem and the adjacent agent subsystem, an adaptive NTSM control strategy of a single driving wheel agent subsystem is obtained. The switch gain of the controller can be adjusted adaptively to compensate for the influence of uncertainty in the system and external disturbances and avoid the chattering and high energy consumption caused by overestimation of the gain. When an agent actuator fails, a Lyapunov function based on the multiagent theory is designed so that the agent can adapt to the new environment and continue to work autonomously without causing the entire system to fall into a fault state.

The simulation results show that under the conditions of limited computing resources, uncertainty and actuator failures, this method is able to coordinate the slip limit problem

of each drive wheel agent subsystem of a distributed driven EV effectively. In addition, driving ability and stability of the vehicle under complex conditions are improved. The maximum speed of a single road condition can be up to 140km/h. The initial velocity of vehicle on wet cobblestone road accelerates from ${}^{0m}/_{s^2}$ to ${}^{3m}/_{s^2}$ within a time of 0.5s. The tracking time of the optimal slip rate of the current road surface under the conditions of different initial slip rates for the four wheels within 0.5s. Under the addition of actuator failures, the time of tracking the current optimal slip rate of the road within 1.5s. When the wet cobblestone road enters the dry cement ground, longitudinal acceleration is maintained after a short adjustment, which ensures the stable driving attitude of the vehicle with good anti- interference performance.

REFERENCES

[1] H. Mirzaeinejad, "Robust predictive control of wheel slip in antilock braking systems based on radial basis function neural network," *Appl. Soft Comput.*, vol. 70, pp. 318–329, Sep. 2018.

[2] M. S. Basrah, E. Siampis, E. Velenis, D. Cao, and S. Longo, "Wheel slip control with torque blending using linear and nonlinear model predictive control," *Vehicle Syst. Dyn.*, vol. 55, no. 11, pp. 1–21, 2017.

[3] D. Tavernini, M. Metzler, P. Gruber, and A. Sorniotti, "Explicit nonlinear model predictive control for electric vehicle traction control," *IEEE Trans. Control Syst. Technol.*, vol. 27, no. 4, pp. 1438–1451, Jul. 2019.

[4] B.-M. Nguyen, S. Hara, H. Fujimoto, and Y. Hori, "Slip control for IWM vehicles based on hierarchical LQR," *Control Eng. Pract.*, vol. 93, Dec. 2019, Art. no. 104179.

[5] B. Zhao, N. Xu, H. Chen, K. Guo, and Y. Huang, "Stability control of electric vehicles with in-wheel motors by considering tire slip energy," *Mech. Syst. Signal Process.*, vol. 118, pp. 340–359, Mar. 2019.

[6] D. Yin, N. Sun, and J.-S. Hu, "A wheel slip control approach integrated with electronic stability control for decentralized drive electric vehicles," *IEEE Trans. Ind. Informat.*, vol. 15, no. 4, pp. 2244–2252, Apr. 2019.

[7] V. Ćirović and D. Aleksendrić, "Adaptive neuro-fuzzy wheel slip control," *Expert Syst. Appl.*, vol. 40, no. 13, pp. 5197–5209, 2013.

[8] G. Yin, S. Wang, and X. Jin, "Optimal slip ratio based fuzzy control of acceleration slip regulation for four-wheel independent driving electric vehicles," *Math. Problems Eng.*, vol. 2013, Nov. 2013, Art. no. 410864.

[9] H. Jing, F. Jia, and Z. Liu, "Multi-objective optimal control allocation for an over-actuated electric vehicle," *IEEE Access*, vol. 6, pp. 4824–4833, 2018.

[10] C. Lin and Z. Xu, "Wheel torque distribution of four-wheel-drive electric vehicles based on multi-objective optimization," *Energies*, vol. 8, no. 5, pp. 3815–3831, Apr. 2015.

[11] H. Fujimoto and S. Harada, "Model-based range extension control system for electric vehicles with front and rear driving–braking force distributions," *IEEE Trans. Ind. Electron.*, vol. 62, no. 5, pp. 3245–3254, May 2015.

[12] S. H. Park, J. S. Kim, J. J. Choi, and H. Yamazaki, "Modeling and control of adhesion force in railway rolling stocks," *IEEE Control Syst. Mag.*, vol. 28, no. 5, pp. 44–58, Oct. 2008.

[13] H. He, J. Peng, R. Xiong, and H. Fan, "An acceleration slip regulation strategy for four-wheel drive electric vehicles based on sliding mode control," *Energies*, vol. 7, no. 6, pp. 3748–3763, Jun. 2014.

[14] R. de Castro, R. E. Araujo, and D. Freitas, "Wheel slip control of EVs based on sliding mode technique with conditional integrators," *IEEE Trans. Ind. Electron.*, vol. 60, no. 8, pp. 3256–3271, Aug. 2013.

[15] A. Zirek, P. Voltr, M. Lata, and J. Novák, "An adaptive sliding mode control to stabilize wheel slip and improve traction performance," *Proc. Inst. Mech. Eng., F, J. Rail Rapid Transit*, vol. 232, no. 10, pp. 2392–2405, Nov. 2018.

[16] J. Zhang and J. Li, "Adaptive backstepping sliding mode control for wheel slip tracking of vehicle with uncertainty observer," *Meas. Control*, vol. 51, nos. 9–10, pp. 396–405, Nov. 2018.

[17] A. M. Boopathi and A. Abudhahir, "Adaptive fuzzy sliding mode controller for wheel slip control in antilock braking system," *J. Eng. Res.*, vol. 4, no. 2, p. 18, Apr. 2016.

[18] L. Yang, J. W. Zhang, and K. H. Guo, "Distribution of driving force and braking force among axles of four-wheel drive electric vehicles," *J. Jilin Univ.*, vol. 45, no. 3, pp. 703–710, 2015.

[19] S. De Pinto, C. Chatzikomis, A. Sorniotti, and G. Mantriota, "Comparison of traction controllers for electric vehicles with on-board drivetrains," *IEEE Trans. Veh. Technol.*, vol. 66, no. 8, pp. 6715–6727, Aug. 2017.

[20] D. Savitski, D. Schleinin, V. Ivanov, and K. Augsburg, "Robust continuous wheel slip control with reference adaptation: Application to the brake system with decoupled architecture," *IEEE Trans. Ind. Informat.*, vol. 14, no. 9, pp. 4212–4223, Sep. 2018.

[21] L. De Novellis, A. Sorniotti, and P. Gruber, "Wheel torque distribution criteria for electric vehicles with torque-vectoring differentials," *IEEE Trans. Veh. Technol.*, vol. 63, no. 4, pp. 1593–1602, May 2014.

[22] Y. Luo, Y. Hu, F. Jiang, R. Chen, and Y. Wang, "Active fault-tolerant control based on multiple input multiple output-model free adaptive control for four wheel independently driven electric vehicle drive system," *Appl. Sci.*, vol. 9, no. 2, p. 276, Jan. 2019.

[23] M. Salehifar, M. Moreno-Eguilaz, G. Putrus, and P. Barras, "Simplified fault tolerant finite control set model predictive control of a five-phase inverter supplying BLDC motor in electric vehicle drive," *Electr. Power Syst. Res.*, vol. 132, pp. 56–66, Mar. 2016.

[24] X. Shao, F. Naghdy, H. Du, and H. Li, "Output feedback H_∞ control for active suspension of in-wheel motor driven electric vehicle with control faults and input delay," *ISA Trans.*, vol. 92, pp. 94–108, Sep. 2019.

[25] T. Chen, L. Chen, X. Xu, Y. Cai, H. Jiang, and X. Sun, "Passive actuator-fault-tolerant path following control of autonomous ground electric vehicle with in-wheel motors," *Adv. Eng. Softw.*, vol. 134, pp. 22–30, Aug. 2019.

[26] T. Roubache, S. Chaouch, and M. S. N. Said, "Sensorless fault-tolerant control of an induction motor based electric vehicle," *J. Electr. Eng. Technol.*, vol. 11, no. 5, pp. 1423–1432, Sep. 2016.

[27] B. Tabbache, M. E. H. Benbouzid, A. Kheloui, and J.-M. Bourgeot, "Virtual-sensor-based maximum-likelihood voting approach for fault-tolerant control of electric vehicle powertrains," *IEEE Trans. Veh. Technol.*, vol. 62, no. 3, pp. 1075–1083, Mar. 2013.

[28] H. Zhang, W. Zhao, and J. Wang, "Fault-tolerant control for electric vehicles with independently driven in-wheel motors considering individual driver steering characteristics," *IEEE Trans. Veh. Technol.*, vol. 68, no. 5, pp. 4527–4536, May 2019.

[29] B. Li, H. Du, and W. Li, "Fault-tolerant control of electric vehicles with in-wheel motors using actuator-grouping sliding mode controllers," *Mech. Syst. signal Process.*, vol. 72, pp. 462–485, May 2016.

[30] D. Zhang, G. Liu, H. Zhou, and W. Zhao, "Adaptive sliding mode fault-tolerant coordination control for four-wheel independently driven electric vehicles," *IEEE Trans. Ind. Electron.*, vol. 65, no. 11, pp. 9090–9100, Nov. 2018.

[31] T. Sun, L. Cheng, W. Wang, and Y. Pan, "Semiglobal exponential control of Euler–Lagrange systems using a sliding-mode disturbance observer," *Automatica*, vol. 112, Feb. 2020, Art. no. 108677.

[32] P. S. Fang, "Chattering reduction method based on switched sliding mode control," *Control Decis.*, vol. 32, no. 7, pp. 1210–1216, 2017.

[33] C. Sun and G. Gong, "Sliding mode control with adaptive fuzzy immune feedback reaching law," *Int. J. Control, Automat. Syst.*, vol. 18, no. 2, pp. 363–373, Feb. 2020.

[34] H. Huang, M. Z. A. Bhuiyan, Q. Tu, C. Jiang, J. Xue, P. Ming, and P. Li, "Fuzzy sliding mode control of servo control system based on variable speeding approach rate," *Soft Comput.*, vol. 23, no. 24, pp. 13477–13487, Dec. 2019.

[35] G. Wang, J. Wu, B. Zeng, Z. Xu, and X. Ma, "A chattering-free sliding mode control strategy for modular high-temperature gas-cooled reactors," *Ann. Nucl. Energy*, vol. 133, pp. 688–695, Nov. 2019.

[36] M. Asad, M. Ashraf, S. Iqbal, and A. I. Bhatti, "Chattering and stability analysis of the sliding mode control using inverse hyperbolic function," *Int. J. Control, Autom. Syst.*, vol. 15, no. 6, pp. 2608–2618, Dec. 2017.

[37] A. Benamor, W. Boukadida, and H. Messaoud, "Genetic algorithm-based multi-objective design of optimal discrete sliding mode approach for trajectory tracking of nonlinear systems," *Proc. Inst. Mech. Eng., C, J. Mech. Eng. Sci.*, vol. 233, no. 15, pp. 5237–5252, Aug. 2019.

[38] P. Li, X. Yu, and B. Xiao, "Adaptive quasi-optimal higher order sliding-mode control without gain overestimation," *IEEE Trans. Ind. Informat.*, vol. 14, no. 9, pp. 3881–3891, Sep. 2018.

[39] Y. Wang, Y. Xia, H. Shen, and P. Zhou, "SMC design for robust stabilization of nonlinear markovian jump singular systems," *IEEE Trans. Autom. Control*, vol. 63, no. 1, pp. 219–224, Jan. 2018.

[40] Y. Wang, P. Shi, Q. Wang, and D. Duan, "Exponential H_∞ filtering for singular Markovian jump systems with mixed mode-dependent time-varying delay," *IEEE Trans. Circuits Syst. I, Reg. Papers*, vol. 60, no. 9, pp. 2440–2452, Sep. 2013.
[41] W.-Y. Wang, M.-C. Chen, and S.-F. Su, "Hierarchical fuzzy-neural control of anti-lock braking system and active suspension in a vehicle," *Automatica*, vol. 48, no. 8, pp. 1698–1706, Aug. 2012.

NIAONA ZHANG received the B.S. and M.S. degrees in power electronics and power transmission from the Changchun University of Technology, Changchun, China, in 1994 and 1999, respectively, and the Ph.D. degree in power electronics and power transmission from the Harbin Institute of Technology, Changchun, in 2006. She held a postdoctoral position with the National Key Laboratory of Automobile Simulation and Control, Jilin University. Since 2011, she has been a Professor with the Changchun University of Technology. Her current research interests include vehicle dynamics control and sliding mode variable structure control.

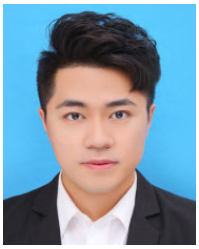

ZONGZHI HAN received the B.S. degree in electrical engineering from Liaoning Shihua University, Fushun, China, in 2016, and the M.S. degree in electrical engineering from the Changchun University of Technology, Changchun, China, in 2020. He is currently pursuing the Ph.D. degree with Jilin University, Changchun. His current research interests include intelligent tires and autonomous vehicles.

ZHE ZHANG received the B.S. and M.S. degrees in control theory and control engineering from the Changchun University of Technology, Changchun, China, in 2011 and 2015, respectively. She is currently pursuing the Ph.D. degree with Jilin University, Changchun.

Her current research interests include vehicle dynamics and control, energy management, and autonomous vehicles.

KONGHUI GUO received the B.S. degree from the Jilin University of Technology, Changchun, China, in 1956.

Since 1994, he has been an Academician with the Chinese Academy of Engineering. He is currently with the National Automobile Dynamic Simulation Laboratory, Jilin University, Changchun. He received seven prizes of the Progress in Science and Technology from the Chinese Government and the National Automatic Industry Corporation, China. His research interests include modeling and simulation of vehicle dynamics, tire dynamics, and vehicle handling and stability.

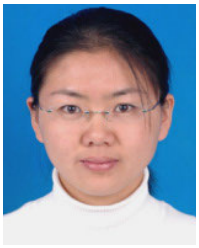

XIAOHUI LU was born in Jilin, China. She received the B.S. degree in mathematics and applied mathematics from Beihua University, Jilin, in 2004, the M.S. degree in operational research and cybernetics from the Lanzhou University of Technology, Lanzhou, China, in 2007, and the Ph.D. degree in control theory and application from Jilin University, Changchun, China, in 2013. She was a Visiting Scholar with the School of College of Engineering, The Ohio State University, under the supervision of Junmin Wang, from 2017 to 2018. Her current research interests include vehicle powertrain control, model predictive control, data-driven control, and triboelectric nanogenerators.